Acta Crystallographica Section D
**Biological Crystallography**
ISSN 0907-4449

# The structure of the ARE-binding domains of Hu antigen R (HuR) undergoes conformational changes during RNA binding

**Hong Wang,[a,b] Fuxing Zeng,[a,b] Qiao Liu,[a,b] Huihui Liu,[a,b] Zexian Liu,[a] Liwen Niu,[a,b] Maikun Teng[a,b]* and Xu Li[a,b]***

[a]School of Life Sciences, University of Science and Technology of China, 96 Jinzhai Road, Hefei, Anhui 230026, People's Republic of China, and [b]Key Laboratory of Structural Biology, Chinese Academy of Sciences, 96 Jinzhai Road, Hefei, Anhui 230026, People's Republic of China

Correspondence e-mail: mkteng@ustc.edu.cn, sachem@ustc.edu.cn

Received 25 May 2012
Accepted 21 November 2012

**PDB References:** ARE-binding domains of HuR, 4egl; RNA-bound, 4ed5

Human RNA-binding protein (HuR), a ubiquitously expressed member of the Hu protein family, plays an important role in mRNA degradation and has been implicated as a key post-transcriptional regulator. HuR contains three RNA-recognition motif (RRM) domains. The two N-terminal tandem RRM domains can selectively bind AU-rich elements (AREs), while the third RRM domain (RRM3) contributes to interactions with the poly-A tail of target mRNA and other ligands. Here, the X-ray structure of two methylated tandem RRM domains (RRM1/2) of HuR in their RNA-free form was solved at 2.9 Å resolution. The crystal structure of RRM1/2 complexed with target mRNA was also solved at 2.0 Å resolution; comparisons of the two structures show that HuR RRM1/2 undergoes conformational changes upon RNA binding. Fluorescence polarization assays (FPA) were used to study the protein–RNA interactions. Both the structure and the FPA analysis indicated that RRM1 is the primary ARE-binding domain in HuR and that the conformational changes induce subsequent contacts of the RNA substrate with the inter-domain linker and RRM2 which greatly improve the RNA-binding affinity of HuR.

## 1. Introduction

The growth and development of eukaryotic organisms require exquisite regulation of gene expression. mRNA decay is one of the major controls of gene expression. In mammalian cells, mRNA decay is tightly regulated by specific *cis*-regulatory sequences and *trans*-acting factors (Bevilacqua *et al.*, 2003). The most frequent and widespread *cis*-regulatory elements of mRNA decay are represented by the adenylate- and uridylate-rich elements (AREs) located in the 3′-untranslated regions (UTRs); they are specifically bound by RNA-binding proteins and finally determine whether mRNA decay is delayed or is facilitated (Eberhardt *et al.*, 2007). Based on the number and the distribution of AUUUA pentamers, AREs have been divided into three classes. Class I AREs contain several dispersed copies of the AUUUA motif within U-rich regions. Class II AREs possess at least two overlapping UUAUU-UA(U/A)(U/A) nonamers. In contrast, the class III AREs are U-rich regions that contain no pentameric AUUUA motif (Barreau *et al.*, 2005). The best characterized ARE-directed mRNA-decay factors include Hu antigen R (HuR; a member of the Hu protein family) and its mutual counteracting regulator ARE/poly-U-binding degradation factor 1 (AUF1, also known as hnRNP D).

The RNA-binding protein HuR is a ubiquitously expressed ~36 kDa protein functionally involved in the stabilization of a number of ARE-containing labile mRNAs coding for cell-cycle regulators, cytokines, growth factors, tumour

suppressors, proto-oncogenes, apoptosis regulatory proteins and various inflammatory enzymes (Doller *et al.*, 2008). HuR predominantly localizes in the nucleus but shuttles between the nucleus and cytoplasm, and has been implicated in the regulation of the stability and translation of over 100 mRNAs in mammalian cells (Meisner & Filipowicz, 2011). HuR contains three RNA-recognition motifs (RRMs): two tandem N-terminal RRM domains (RRM1 and RRM2) that recognize U-rich hairpin-loops with high affinity (Uren *et al.*, 2011) and all types of AREs of target mRNA molecules (Fan & Steitz, 1998), and a third RRM domain (RRM3) that contributes to interactions with the poly-A tail of target mRNA and other ligands (Güttinger *et al.*, 2004). RRM3 has also been reported to have a terminal adenosyltransferase activity and to be indispensable for the mRNA-stabilizing ability of HuR (Meisner *et al.*, 2009). A specific HuR nucleo-cytoplasmic shuttling sequence (HNS) located in the long hinge region between its second and third RRMs may enable HuR to translocate from the nucleus into the cytoplasm in order to stabilize and/or enhance the translational efficiency of its target mRNAs (Brennan & Steitz, 2001). Among the various ARE-binding proteins known to date, HuR is still the only known ubiquitous antagonist of post-transcriptional gene silencing by AREs. Given the wide-ranging repertoire of known and suspected targets of HuR, it is considered to be a central node in the ARE pathway (Benoit *et al.*, 2010). In contrast to HuR, the other members of the Hu family (HuB, HuC and HuD) show strict tissue-specific characteristics: HuB is found in neurons and gonads, and the expression of HuC and HuD is restricted to neurons (Deschênes-Furry *et al.*, 2006). Homodimerization is necessary for the physiological function of all Hu proteins (Meisner *et al.*, 2007). Interestingly, HuB, HuC and HuD may form homodimers *via* the third RRM (Kasashima *et al.*, 2002), whereas HuR forms homodimers *via* a disulfide bond formed by the N-terminal Cys13 residue (Benoit *et al.*, 2010).

To date, structures of N-terminal tandem RRM domains have been solved for two members of the vertebrate Hu protein family: the solution structure of house mouse HuC RRM1/2 complexed with RNA (PDB entry 1fnx; M. Inoue, M. Hirao, K. Kasashima, I.-S. Kim, G. Kawai, T. Kigawa, H. Sakamoto, Y. Muto & S. Yokoyama, unpublished work) and crystal structures of *Homo sapiens* HuD RRM1/2 complexed with target RNA sequences (Harada *et al.*, 2007). Previous SAXS data analysis for HuR revealed that HuR RRM1/2 binds RNA with a closed globular conformation, which is significantly different to the open/flexible conformation of its RNA-free form (Kim *et al.*, 2011). Owing to the lack of comparable crystal structures of HuR RRM1/2 and RRM1/2–RNA, the structural details of this conformation change are still unknown. Moreover, although it has been well documented that the primary RNA-binding domain of Hu proteins is RRM1 (Park *et al.*, 2000), structural evidence for this is not available for HuR. To understand how HuR binds and stabilizes ARE-containing mRNAs and how HuR undergoes major conformational changes during the above process, structural investigation of the first two tandem RRM domains (RRM1/2) of HuR and of their complex with target mRNA is of great importance. Here, we report the structures of HuR RRM1/2 and of HuR RRM1/2 complexed with an 11-base segment (5′-AUUUUUAUUUU-3′) of *c-fos* mRNA. Fluorescence polarization assays were carried out to study the protein–RNA interactions. Our structural studies revealed why HuR RRM1 is the critical nucleic acid-binding domain and how HuR tandem RRM1/2 undergoes severe conformational changes to form a stable protein–RNA complex with higher affinity.

## 2. Materials and methods

### 2.1. Protein expression and purification

Details of the expression, purification and methylation of wild-type recombinant HuR RRM1/2 (residues 18–186) have been described in a previous publication (Wang *et al.*, 2011). HuR RRM1 (residues 18–99) and HuR RRM2 (residues 105–186) were cloned as His-tag fusion proteins into pET22b vector (Novagen). Mutants of HuR RRM1/2 were obtained using the PCR protocol in the MutanBEST kit (Takara). All of the plasmids were confirmed by DNA sequencing. RRM1, RRM2 and all of the mutants were prepared using the same methods as used for the wild-type protein. For preparation of the RNA–RRM1/2 complex, native HuR RRM1/2 was further purified by HiTrap SP FF cation-exchange chromatography (GE Healthcare) and was then dialyzed against buffer *A* (10 m*M* HEPES pH 7.0, 200 m*M* NaCl, 0.1 m*M* EDTA, 5% glycerol).

### 2.2. Crystallization and data collection

The methylated HuR RRM1/2 protein at a concentration of 9 mg ml$^{-1}$ in buffer *B* (20 m*M* Tris pH 7.5, 200 m*M* NaCl) was crystallized at 287 K using the hanging-drop vapour-diffusion method by mixing 1 µl protein solution and 1 µl reservoir solution and equilibrating the drop against 200 µl reservoir solution. Crystals were obtained using a reservoir solution consisting of 1.5 *M* $Li_2SO_4$, 0.1 *M* Tris pH 8.5. For preparation of the RNA complex, native RRM1/2 in buffer *A* was incubated with AUUUUUAUUUU (Takara) (RNA:protein ratio of 1.2:1.0) on ice for 0.5 h, with a final protein concentration of approximately 9 mg ml$^{-1}$. The RRM1/2–RNA complex was crystallized at 287 K using a hanging-drop vapour-diffusion method indentical to that used for methylated HuR RRM1/2. Crystals of the protein–RNA complex were obtained using a reservoir solution consisting of 18% MPEG5000, 0.1 *M* HEPES pH 7.5. For data collection, crystals were transferred into a cryoprotectant solution that consisted of the reservoir solution supplemented with an additional 25%(*v*/*v*) glycerol. X-ray diffraction data were collected on beamline 17U1 at Shanghai Synchrotron Radiation Facility (SSRF) and were subsequently processed using *HKL*-2000 (Otwinowski & Minor, 1997).

### 2.3. Structure determination

The HuR RRM1/2 crystals belonged to space group $P2_12_12$, with unit-cell parameters $a$ = 41.18, $b$ = 132.72, $c$ = 31.10 Å.

**Table 1**
Data-collection and refinement statistics for HuR RRM1/2.

| | RRM1/2 | RRM1/2–RNA |
|---|---|---|
| Data collection | | |
| Space group | $P2_12_12$ | $C2$ |
| Unit-cell parameters (Å, °) | $a$ = 41.18, $b$ = 132.72, $c$ = 31.10 | $a$ = 136.77, $b$ = 62.75, $c$ = 53.29, $\alpha = \gamma = 90$, $\beta$ = 111.89 |
| Wavelength (Å) | 0.9999 | 0.9979 |
| Resolution (Å) | 50–2.90 (3.00–2.90) | 35.08–2.00 (2.11–2.00) |
| Unique reflections | 4062 | 27777 |
| Completeness (%) | 97.3 (92.9) | 98.4 (98.9) |
| Multiplicity | 3.5 (3.4) | 3.5 (3.3) |
| Average $I/\sigma(I)$ | 12.4 (2.3) | 6.4 (4.8) |
| $R_{merge}$ (%) | 9.4 (46.5) | 15.2 (16.3) |
| Refinement statistics | | |
| $R_{work}/R_{free}$ (%) | 26.5/29.4 | 21.1/25.7 |
| No. of water molecules | | 252 |
| R.m.s.d. bond lengths (Å) | 0.009 | 0.010 |
| R.m.s.d. bond angles (°) | 1.259 | 1.217 |
| Average $B$ factors (Å$^2$) | 59.7 | 22.9 |
| Ramachandran analysis (%) | | |
| Most favoured regions | 90.5 | 96.0 |
| Additional allowed regions | 9.5 | 3.7 |
| Disallowed regions | 0 | 0 |
| PDB code | 4egl | 4ed5 |

Each asymmetric unit contained one HuR RRM1/2 molecule. The structure was solved to 2.9 Å resolution by the molecular-replacement method using the isolated RRM1 and RRM2 domains of HuD RRM1/2 (PDB entry 1fxl; Harada *et al.*, 2007) as search models in *Phaser* (Storoni *et al.*, 2004). Refinement was performed by *REFMAC*5 (Murshudov *et al.*, 2011). Between each round of refinement, the model was fitted to the $2F_o - F_c$ electron-density map with the program *Coot* (Emsley & Cowtan, 2004). The translation–libration–screw (TLS) model was used near the end of refinement. The final refined model had an $R$ factor of 26.5% and an $R_{free}$ of 29.4%. The quality of the final model was checked with *PROCHECK* (Laskowski *et al.*, 1996). The HuR RRM1/2–RNA crystals belonged to space group $C2$, with unit-cell parameters $a$ = 136.77, $b$ = 62.75, $c$ = 53.29 Å, $\alpha = \gamma = 90$, $\beta$ = 111.89°. Each asymmetric unit contained two copies of the HuR RRM1/2–DNA complex. Phases were again determined by molecular replacement with *Phaser* (Storoni *et al.*, 2004) using the isolated RRM1 and RRM2 domains of the RNA-free form of HuR RRM1/2 as search models. Two RNA molecules could be traced in the electron-density map and their RNA chains were manually added by fitting to $2F_o - F_c$ and $F_o - F_c$ density maps in *Coot* (Emsley & Cowtan, 2004). *REFMAC*5 was used for refinement (Murshudov *et al.*, 2011). Water molecules were added to the model in the final stages. Near the end of refinement the TLS model was also applied. The final refined model had an $R$ factor of 21.1% and an $R_{free}$ of 25.7% and was validated using *PROCHECK* (Laskowski *et al.*, 1996).

The detailed final refinement statistics are given in Table 1. It is noticeable that the $R_{merge}$ and $I/\sigma(I)$ of the HuR–RNA complex are unusual in that the value in the highest resolution shell is almost the same as the overall average. This problem arose from some technical issues in collecting the data and we did not harvest the higher resolution spots. Since we were not able to obtain any further crystals in order to collect a better diffraction data set and this data set gives a normal Wilson plot, we provide these data here. Figures were prepared using *PyMOL* (http://www.pymol.org).

### 2.4. Fluorescence polarization assays

The sequence of the fluorescently labelled (5′-FAM) RNA probe is AUUUUUAUUUU. Fluorescence polarization assays were performed in Tris–HCl buffer (20 m*M* Tris pH 8.0, 200 m*M* NaCl, 5% glycerol) at 293 K using a SpectraMax M5 microplate-reader system. The wavelengths of fluorescence excitation and emission were 490 and 522 nm, respectively. Each well of a 384-well plate contained 80 n*M* 5′-FAM RNA probe and different concentrations of HuR RRM1/2 with a final volume of 80 µl. For each assay, RNA-free controls were included. The fluorescence polarization $P$ (in mP units) was calculated using the equation $P = (I_{\parallel} - I_{\perp})/(I_{\parallel} + I_{\perp})$. The fluorescence polarization change $\Delta P$ (in mP units) was fitted to the equation $\Delta P = \Delta P_{max} \times [\text{protein}]/(K_d + [\text{protein}])$.

### 2.5. Electrostatic free-energy analysis

An electrostatic free-energy analysis was conducted with *DelPhi* (Li *et al.*, 2012). For calculations, structure files were prepared from the apo (HuR RRM1/2 RNA-free form; PDB entry 4egl, chain $A$ residues 18–171) and holo (HuR RRM1/2 RNA-bound form; PDB entry 4ed5, chain $A$ residues 18–171 and chain $D$ residues 2–11) proteins and H atoms were added using the *Reduce* software (Word *et al.*, 1999). The binding energy (P, protein; R, RNA; PR, protein + RNA) was calculated as

$$\Delta G^{\text{binding}} = \Delta G^{\text{coulombic}} + \Delta\Delta G^{\text{reaction-field}} + \Delta\Delta G^{\text{ions}}, \quad (1)$$

where

$$\Delta G^{\text{coulombic}} = G_{\text{PR}}^{\text{coulombic}} - G_{\text{P}}^{\text{coulombic}} - G_{\text{R}}^{\text{coulombic}}, \quad (2)$$

$$\Delta\Delta G^{\text{reaction-field}} = \Delta G_{\text{PR}}^{\text{reaction-field}} - \Delta G_{\text{P}}^{\text{reaction-field}} - \Delta G_{\text{R}}^{\text{reaction-field}}, \quad (3)$$

$$\Delta\Delta G^{\text{ions}} = \Delta G_{\text{PR}}^{\text{ions}} - \Delta G_{\text{P}}^{\text{ions}} - \Delta G_{\text{R}}^{\text{ions}}. \quad (4)$$

The binding energies were 465.55 and 208.16 kJ mol$^{-1}$ for the apo and holo proteins, respectively, at a salt concentration of 0.2 *M*. The free energy of the apo-to-holo transition for the protein is thus estimated as 257.39 kJ mol$^{-1}$. The solvation energies (reaction-field energies) for the apo and holo proteins were −2278.72 and −2086.93 kJ mol$^{-1}$, respectively.

## 3. Results and discussion

### 3.1. Overall structure of RNA-free HuR RRM1/2

We constructed plasmids for full-length HuR and for the RRM1/2 segment (residues 18–186) and the RRM3 segment (residues 242–322) of recombinant HuR. However, owing to the poor solubility and stability problems of full-length HuR and its RRM3 segment, only RRM1/2 (residues 18–186) could be purified for crystallization. Native protein (RRM1/2) could

be crystallized, but none of the crystals gave rise to diffraction of sufficient quality. Several parameters (such as temperature, pH and buffer) were changed to optimize the crystallization, but only lysine methylation was successful in generating crystals. A diffraction data set was collected to 2.9 Å resolution for methylated HuR RRM1/2.

The crystal structure of methylated HuR RRM1/2 was solved by molecular replacement. The refined model reported here contains residues Gly18–Ala184 of one RRM1/2 molecule in the asymmetric unit. Owing to poor electron density, two regions were not modelled in the final structure. These regions included Pro172 and Pro173, which reside in loop 5 of RRM2, together with the last ten residues at the C-terminus. Both of the two HuR RRM domains adopt the canonical $\alpha\beta$-sandwich structure with a typical $\beta1$–$\alpha1$–$\beta2$–$\beta3$–$\alpha2$–$\beta4$ topology, as expected from sequence homology with other RRM-containing proteins. The central regions of the $\beta1$ and $\beta3$ strands contain the conserved RNP2 and RNP1 motifs, respectively. Superimposition of HuR RRM1 and RRM2 shows a root-mean-square difference (r.m.s.d.) of 0.92 Å for 67 $C^{\alpha}$ positions (Fig. 1*b*). Loop 5 connecting $\alpha2$ and $\beta4$ in RRM1 adopts a common $\beta$–turn–$\beta$ conformation which does not exist in the same position of RRM2.

Unlike the structures of other tandem RRM domains, the crystal structure of HuR RRM1/2 reveals an open conformation with no inter-domain contacts between the two RRM domains. The 12-residue inter-domain linker (Tyr95–Ala106) forms a short $3_{10}$-helix and maintains the distance between the two RRM domains at greater than 13 Å (Fig. 1*a*).

### 3.2. Overall structure of the HuR RRM1/2–RNA complex

The HuR RRM1/2–RNA complex crystals belonged to space group *C*2. Each asymmetric unit contained two copies of a 1:1 RRM1/2–RNA complex. In the following, we describe one of the two complexes in the asymmetric unit (Figs. 2*a* and 2*c*). The protein folds of both RRM domains are similar to those in the free form, with r.m.s.d.s of 0.39 Å (67 $C^{\alpha}$ positions) for RRM1 and 0.48 Å (64 $C^{\alpha}$ positions) for RRM2. In contrast to the open conformation of the free form of RRM1/2, the HuR RRM1/2 in the RRM1/2–RNA complex presents a closed shape in which the two RRM domains form a positively charged cleft for RNA binding (Fig. 2*b*). The closed conformation results in new interactions between the two RRM domains (the side chain of Lys92 hydrogen-bonds to the main-chain carbonyl O atom of Ile133) and between RRM2 and the inter-domain linker (the main-chain carbonyl O atom and OD1 atoms of Asp155 interact with the NH1 atom of Arg97, and the main-chain carbonyl O atom of Val102 interacts with the main-chain N atom) as in the HuD complex structure. These hydrogen-bond interactions do not exist in the free form of HuR RRM1/2 owing to its open conformation.

Eight nucleotides from U3 to U10 and the 5′ phosphate and ribose ring of U11 were visible in this protein–RNA complex. The conformation of the RNA chain is similar to that in the HuD–RNA complex (PDB entry 1fxl), with a turn at U5. Although the RNA-recognition mode is also similar in HuR and HuD, there are some differing protein–RNA contacts (Fig. 3). Several interactions that are present in the HuR–RNA complex do not exist in HuD–RNA: (i) the main-chain N atom of Ala185 forms a hydrogen bond to the O atom of U3; (ii) Leu61 (the methyl groups in the side chain) provides a hydrophobic environment for A7 and the main-chain carbonyl O atom of Leu61 makes hydrogen-bond interactions with the 2′-OH of A7; (iii) the NH1 atom of Arg153 (the position equivalent to Arg172 in HuD) also interacts with the 2′-OH of U8 in addition to forming a hydrogen bond with the phosphate group and (iv) the NZ atom of Lys104 and the main-chain carbonyl O atom of Ser100 interact with the phosphate group

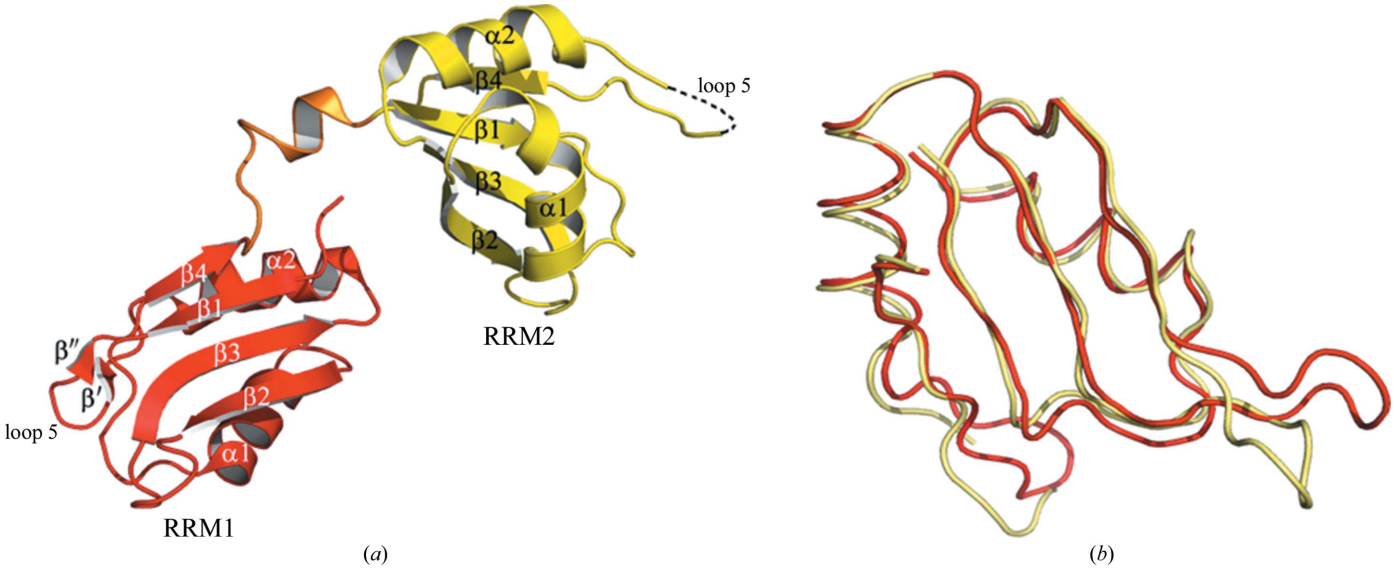


**Figure 1**
Structure of HuR RRM1/2. HuR RRM1 and RRM2 are coloured red and yellow, respectively. (*a*) Overview of HuR RRM1/2. (*b*) Superposition of HuR RRM1 and RRM2 shows the structural similarity between the two RRM domains.

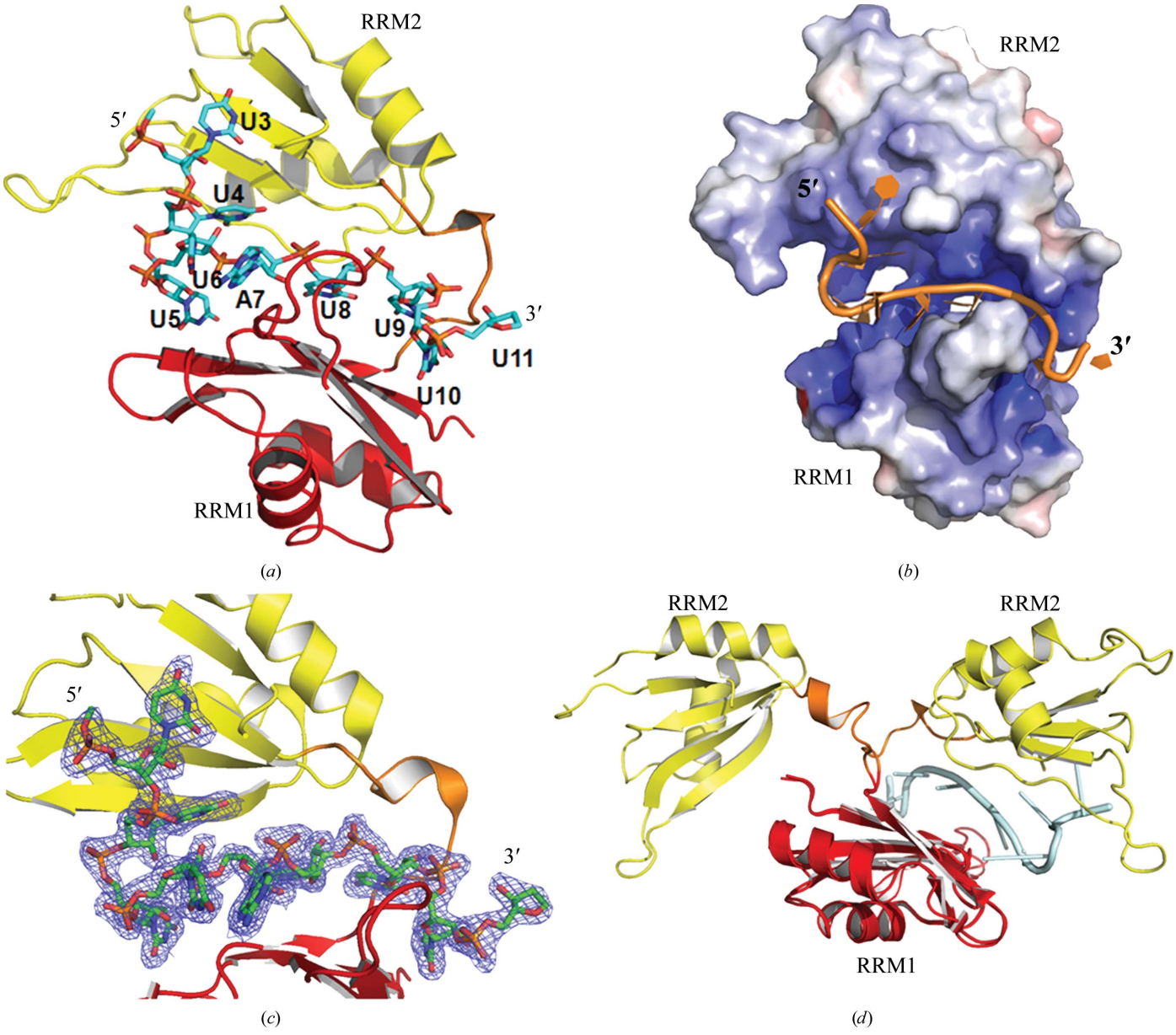


**Figure 2**
(*a*) Structure of the HuR RRM1/2–RNA complex. All of the RNA bases are labelled. (*b*) The RNA element is located in a positively charged cavity formed by HuR RRM1 and RRM2. Positive charges and negative charges are coloured blue and red, respectively. (*c*) View of the RNA element covered with a $2F_o - F_c$ electron-density map contoured at $1\sigma$. The RNA element is shown in ball-and-stick representation. (*d*) Superposition of RRM1 from the RNA-free and RNA-bound forms of HuR RRM1/2. The RRM1 and RRM2 domains and the RNA element are coloured red, yellow and cyan, respectively.

and 2′-OH of U9, respectively. Details of the protein–RNA interactions are shown in Supplementary Fig. 1[1]. There are more atoms of RNA that are recognized through water in the HuR–RNA complex than in the HuD–RNA complex. Previous reports indicate that the 2′-OH groups of RNA substrates are important for their interaction with HuR RRM1/2, such that HuR RRM1/2 preferentially binds U-rich RNA compared with U-rich DNA (Kim *et al.*, 2011). This conclusion is verified by the structure of the RRM1/2–RNA complex, in which several 2′-OH groups are recognized by critical residues in HuR RRM1/2.

### 3.3. HuR RRM1 is the critical nucleic acid-binding domain

To characterize the RNA-binding properties of HuR RRM1/2, fluorescence polarization assays (FPA) were performed to quantify the RNA-binding affinities of the tandem RRM domains (RRM1/2) and each individual RRM

[1] Supplementary material has been deposited in the IUCr electronic archive (Reference: BE5209). Services for accessing this material are described at the back of the journal.

domain (RRM1 or RRM2). As shown in Fig. 4, HuR RRM1/2 bound to the 11-base AU-rich segment with a $K_d$ value of about 169 n*M*, compared with an RNA-binding affinity of 4.88 µ*M* for HuR RRM1 alone. In contrast, RRM2 bound to the RNA with a low affinity that could not be detected by FPA.

In accordance with previous studies, the results of FPA for the individual RRM domains indicate that RRM1 is the primary ARE-binding domain of HuR. The structure analysis clearly reveals the structural basis of the above phenomenon: in the HuR RRM1/2–RNA complex RRM1 recognizes five nucleotides U5–U8 and U10, while the inter-domain linker interacts with U9 and RRM2 interacts with U3–U4. The ability to recognize four or five consecutive uracil-recognition groups gives RRM1 a strong RNA-binding capacity in solution, whereas the capability of the inter-domain linker and RRM2 to recognise one or two uracils is not sufficient to capture poly-(U) substrate from solution.

Owing to the high sequence identity in the Hu protein family, NMR studies on HuC and SPR experiments on HuD revealed the same RNA-binding properties, which are consistent with the above results (Park *et al.*, 2000; Harrison *et al.*, 1985). In the HuD RRM1/2–RNA complex two individual RRM domains also recognize poly-(U) substrate in the same conserved manner as in HuR.

### 3.4. Severe conformational changes increase the RNA-binding affinity of HuR RRM1/2

The crystal structures of HuR RRM1/2 and its RNA complex present two distinct conformations: an open state (RNA-free form) and a closed state (RNA-bound form). Although the protein folds of the individual RRM domains in the RNA-bound form are essentially the same as those in the RNA-free form, the tertiary structure undergoes dramatic conformational changes upon RNA binding. Superimposition of RRM1 in these two structures shows that HuR RRM2 in the complex has undergone a rotation of 137.3 radians in the direction required to form the RNA-binding cleft (Fig. 2*d*). This conformational change was also observed in a SAXS data analysis of HuR, which indicated that HuR maintained an open/flexible conformation in the RNA-free form in solution and a compact closed conformation in its RNA-bound form

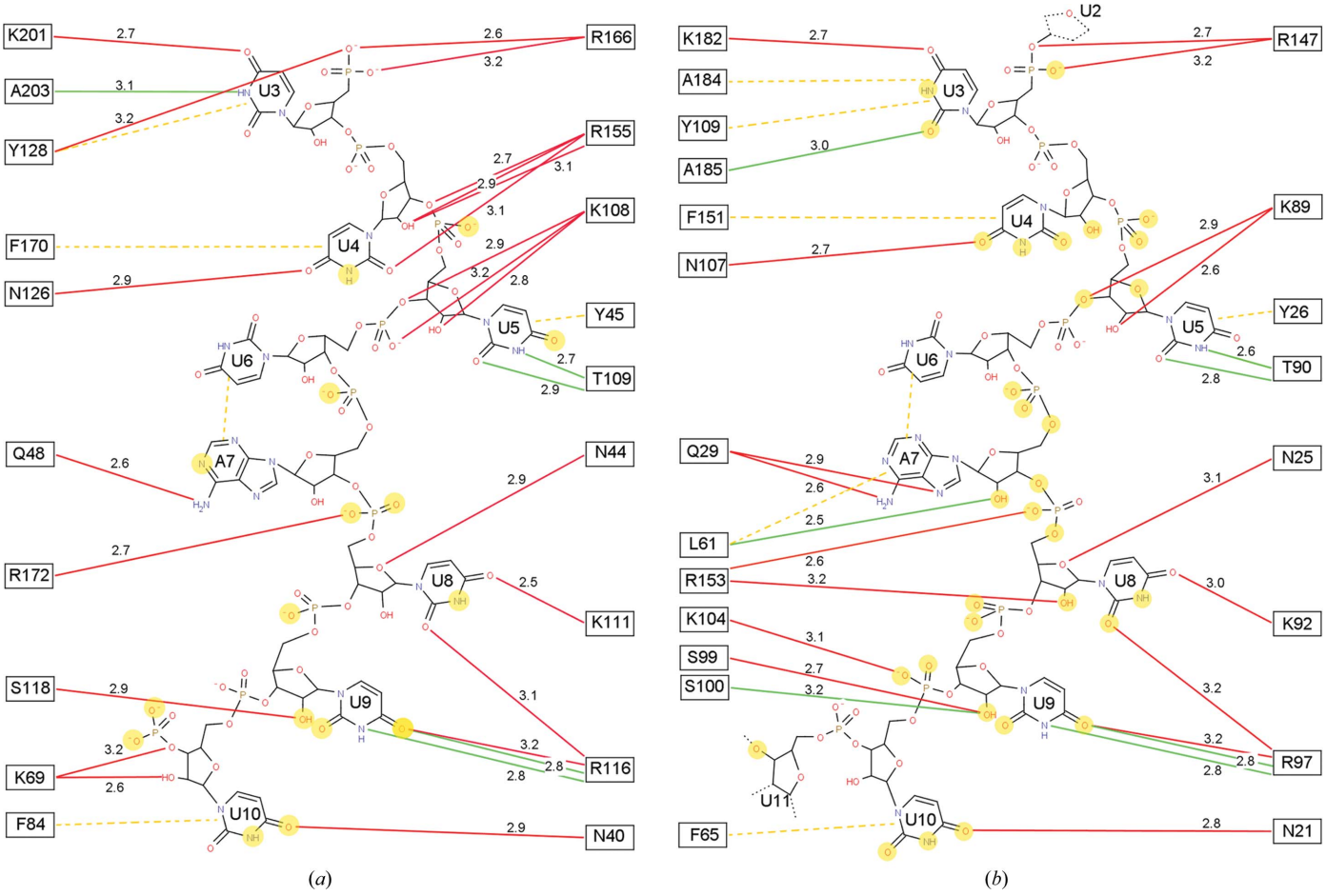


**Figure 3**
Protein–RNA contacts of (*a*) HuD and (*b*) HuR. Red lines show side-chain contacts, green lines show main-chain contacts and dashed orange lines show stacking interactions. Distances are labelled in Å. The RNA atoms that are highlighted in light orange indicate water-mediated contacts. The electron density for the side chain of Lys50 (the position equivalent to Lys69 in HuD) is not well defined. Arg146 (the position equivalent to Arg155 in HuD) recognizes U4 through hydrogen bonds which are mediated by water. Therefore, Lys50 and Arg146 are not shown in (*b*).

(Kim *et al.*, 2011). In the SAXS analysis, the molecular diameters of RNA-bound HuR RRM1/2 calculated using the SAXS method (∼51 Å) are in good agreement with the crystal structure (∼54 Å), which indicates that the results of these two methods are comparable. The molecular diameter of RNA-free HuR RRM1/2 varied from 56 to 74 Å in the SAXS analysis, which indicated that the relative positions of the two RRM domains display a series of changing states under the shackle of the inter-domain linker; our HuR RRM1/2 structure (molecular diameter of ∼64 Å) reveals one momentary state from these abundant open/flexible conformations.

The electrostatic free-energy analysis revealed that while HuR RRM1/2 could retain the closed conformation observed in the RNA-bound complex structure even in the absence of RNA, its free energy would be higher than that of the RNA-free form by about 257 kJ mol$^{-1}$. This result indicates that the closed conformation which was observed in our HuR–RNA complex could probably not spontaneously appear in the open/flexible state. From the open/flexible state (with a solvation energy of −2278.72 kJ mol$^{-1}$) HuR first needs to bind RNA substrate *via* RRM1; the released binding energy would then induce the subsequent conformational changes of the inter-domain linker and RRM2. Finally, HuR RRM1/2 bound to RNA substrate in the compact closed conformation can remain in a more stable energy state (with a solvation energy of −2086.93 kJ mol$^{-1}$). This deduction is consistent with the results of the following FPA experiments.

Similar dramatic conformational changes of tethered-protein domains induced by nucleic acid binding have also been reported for the three zinc fingers of *Xenopus laevis* transcription factor IIIA (TFIIIA; Wuttke *et al.*, 1997) and two RRM domains of *Drosophila melanogaster* sex-lethal protein (SXL; Handa *et al.*, 1999). Two TGEKP (N) linkers and three zinc-finger motifs of TFIIIA maintain a flexible relative position in solution without DNA, but substrate binding induces an ordered compact conformation that fixes the DNA substrate with high affinity. For SXL, two isolated RRM domains and the inter-domain linker aggregate upon RNA binding to form a compact global conformation with a V-shaped RNA-binding cleft which is formed by the $\beta$-sheet platforms of the two RRM domains.

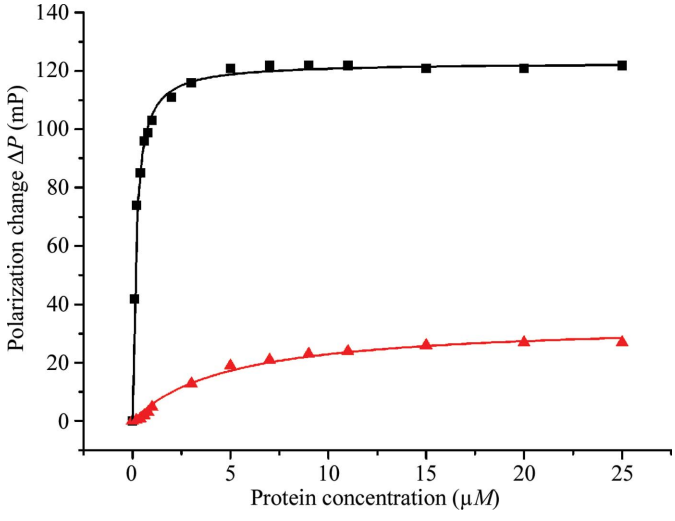


**Figure 4**
RNA-binding analysis by FPA. HuR RRM1/2 (black) and HuR RRM1 (red) bind to 11-base RNA with $K_d$ values of 169 n*M* and 4.88 μ*M*, respectively.

As a result of this conformational change, RRM2 and the inter-domain linker of HuR can subsequently contact the mRNA substrate following its initial recognition by RRM1. This RNA-binding-induced conformational change greatly increases the contact area between HuR and RNA, and also significantly increases the affinity between them. In the HuR–RNA complex structure the whole contact area between HuR and RNA is ∼1262.3 Å$^2$, of which RRM1 contributes 611.3 Å$^2$, the inter-domain linker contributes 229.8 Å$^2$ and RRM2 contributes 459.3 Å$^2$. Although the inter-domain linker and RRM2 bind only three uracil bases, they provide almost half of the contact area between HuR and its RNA substrate. This shows that conformational changes play a very important role in the improvement in affinity between HuR and RNA. To confirm the above inference based on the complex structure, all essential residues which contributed to recognition of the RNA substrate were replaced by alanines. A circular-dichroism (CD) spectral assay was conducted to determine the secondary structures of these mutants. The CD results (data not shown) indicated that the secondary structures of some mutants were changed in comparison with wild-type protein. Therefore, only five mutants (Asn21 and Thr90 in RRM1, Arg97 in the inter-domain linker region and Arg136 and Arg147 in RRM2) were suitable for FPA analysis owing to the changes in solubility and secondary structure. The results of FPA indicated that all five mutants reduced the HuR–RNA binding affinity, with $K_d$ values of 0.50, 0.52, 2.11, 0.86 and 0.73 μ*M*, respectively, suggesting that these residues indeed play a key role in the RNA-binding process. In particular, the R97A mutation showed the highest reduction in affinity, indicating that the inter-domain linker not only contributes to RNA recognition but also influences the subsequent conformation change and RNA binding by RRM2.

## 4. Conclusion

To understand how HuR recognizes ARE-containing mRNAs and how HuR undergoes major conformational changes during the above process, we solved crystal structures of HuR RRM1/2 in an RNA-free form at 2.9 Å resolution and in an RNA-bound form at 2.0 Å resolution. These two structures revealed an open conformation without substrate and a closed conformation with an 11-base RNA. They revealed the structural basis for HuR RRM1/2 recognition and indicated that a dramatical conformation change takes place upon RNA binding during the substrate-binding process. Both structural analysis and FPA analysis indicated that RRM1 is the primary ARE-binding domain in HuR and the conformation change induced subsequent contacts between the inter-domain linker and RRM2 and the RNA substrate which greatly improved the RNA-binding affinity of HuR.

We thank the staff at SSRF beamline BL17U for assistance with synchrotron data collection. Financial support for this project was provided by the Chinese Ministry of Science and Technology (grant Nos. 2012CB917200 and 2009CB825500) and the Chinese National Natural Science Foundation (grant Nos. 31270014, 31130018, 30900224 and 10979039).

## References

Barreau, C., Paillard, L. & Osborne, H. B. (2005). *Nucleic Acids Res.* **33**, 7138–7150.
Benoit, R. M., Meisner, N. C., Kallen, J., Graff, P., Hemmig, R., Cèbe, R., Ostermeier, C., Widmer, H. & Auer, M. (2010). *J. Mol. Biol.* **397**, 1231–1244.
Bevilacqua, A., Ceriani, M. C., Capaccioli, S. & Nicolin, A. (2003). *J. Cell. Physiol.* **195**, 356–372.
Brennan, C. M. & Steitz, J. A. (2001). *Cell. Mol. Life Sci.* **58**, 266–277.
Deschênes-Furry, J., Perrone-Bizzozero, N. & Jasmin, B. J. (2006). *Bioessays*, **28**, 822–833.
Doller, A., Pfeilschifter, J. & Eberhardt, W. (2008). *Cell. Signal.* **20**, 2165–2173.
Eberhardt, W., Doller, A., Akool, el-S. & Pfeilschifter, J. (2007). *Pharmacol. Ther.* **114**, 56–73.
Emsley, P. & Cowtan, K. (2004). *Acta Cryst.* D**60**, 2126–2132.
Fan, X. C. & Steitz, J. A. (1998). *EMBO J.* **17**, 3448–3460.
Güttinger, S., Mühlhäusser, P., Koller-Eichhorn, R., Brennecke, J. & Kutay, U. (2004). *Proc. Natl Acad. Sci. USA*, **101**, 2918–2923.
Handa, N., Nureki, O., Kurimoto, K., Kim, I., Sakamoto, H., Shimura, Y., Muto, Y. & Yokoyama, S. (1999). *Nature (London)*, **398**, 579–585.
Harada, K., Ogata, M. & Mitsunaga, M. (2007). *Opt. Lett.* **32**, 1111–1113.
Harrison, S. C., Winkler, F. K., Schutt, C. E. & Durbin, R. M. (1985). *Methods Enzymol.* **114**, 211–237.
Kasashima, K., Sakashita, E., Saito, K. & Sakamoto, H. (2002). *Nucleic Acids Res.* **30**, 4519–4526.
Kim, H. S., Wilce, M. C. J., Yoga, Y. M. K., Pendini, N. R., Gunzburg, M. J., Cowieson, N. P., Wilson, G. M., Williams, B. R. G., Gorospe, M. & Wilce, J. A. (2011). *Nucleic Acids Res.* **39**, 1117–1130.
Laskowski, R. A., Rullmannn, J. A., MacArthur, M. W., Kaptein, R. & Thornton, J. M. (1996). *J. Biomol. NMR*, **8**, 477–486.
Li, C., Li, L., Zhang, J. & Alexov, E. (2012). *J. Comput. Chem.* **33**, 1960–1966.
Meisner, N. C. & Filipowicz, W. (2011). *Adv. Exp. Med. Biol.* **700**, 106–123.
Meisner, N. C., Hintersteiner, M., Mueller, K., Bauer, R., Seifert, J. M., Naegeli, H. U., Ottl, J., Oberer, L., Guenat, C., Moss, S., Harrer, N., Woisetschlaeger, M., Buehler, C., Uhl, V. & Auer, M. (2007). *Nature Chem. Biol.* **3**, 508–515.
Meisner, N. C., Hintersteiner, M., Seifert, J. M., Bauer, R., Benoit, R. M., Widmer, A., Schindler, T., Uhl, V., Lang, M., Gstach, H. & Auer, M. (2009). *J. Mol. Biol.* **386**, 435–450.
Murshudov, G. N., Skubák, P., Lebedev, A. A., Pannu, N. S., Steiner, R. A., Nicholls, R. A., Winn, M. D., Long, F. & Vagin, A. A. (2011). *Acta Cryst.* D**67**, 355–367.
Otwinowski, Z. & Minor, W. (1997). *Methods Enzymol.* **276**, 307–326.
Park, S., Myszka, D. G., Yu, M., Littler, S. J. & Laird-Offringa, I. A. (2000). *Mol. Cell. Biol.* **20**, 4765–4772.
Storoni, L. C., McCoy, A. J. & Read, R. J. (2004). *Acta Cryst.* D**60**, 432–438.
Uren, P. J., Burns, S. C., Ruan, J., Singh, K. K., Smith, A. D. & Penalva, L. O. (2011). *J. Biol. Chem.* **286**, 37063–37066.
Wang, H., Li, H., Shi, H., Liu, Y., Liu, H., Zhao, H., Niu, L., Teng, M. & Li, X. (2011). *Acta Cryst.* F**67**, 546–550.
Word, J. M., Lovell, S. C., Richardson, J. S. & Richardson, D. C. (1999). *J. Mol. Biol.* **285**, 1735–1747.
Wuttke, D. S., Foster, M. P., Case, D. A., Gottesfeld, J. M. & Wright, P. E. (1997). *J. Mol. Biol.* **273**, 183–206.